

CHAPTER 3

3. EXPERIMENTAL METHOD OF CHARACTERISING CAPPING LAYER PROPERTIES

3.1 Introduction

Deformation of the substructure can be divided into two parts, recoverable elastic deformation which is a measure of the resilient behaviour, and non-recoverable plastic deformation which is a measure of absorbent behaviour. The current characterisation of substructure design and analysis is based on the resilient properties of soil. As such, in the past much emphasis was given to the study of the resilient behaviour of soils, particularly in pavement designs. The use of Resilient Modulus (M_r) as an indicator of the resilient behaviour has been introduced successfully into the design of flexible pavements. The focus of most recent efforts have been on providing better interpretation, understanding and application of M_r into mechanistic design models. A potential parameter which directly governs the plastic deformations is yet to be introduced for practical design considerations.

The current design practice of rail substructure is based on California Bearing Ratio (CBR) and soil bearing capacity. The safe average bearing pressure method (based on static testing techniques applied to saturated soils) and the British Rail formation design method (based on repeated load tests) are the two major methods developed to determine the allowable bearing pressure of the subgrade (Jeffs and Tew, 1991). The experiments such as the CBR test and the repeated load tri-axial test have allowed reliable design procedures but failed to explain global and local failure of the subgrade. Lay (1990) has discussed that, though field bearing tests and CBR tests provide correct in-situ soil strength, they are

slow and cumbersome and only give results specific to the location. Efforts have therefore been made to generalise the available knowledge and experiences using the elastic theories to evaluate the effect of the dynamic and repetitive character of the traffic loading.

Drumm et. al. (1996) introduced an Alternative Resilient Modulus Test Method (ATM) for fine grained soils, based on a falling weight impacting on a Standard Proctor specimen. A falling weight load was used to simulate a moving vehicle and the applied load or stress was controlled by varying the weight and height of fall as shown in Fig. 3.1.

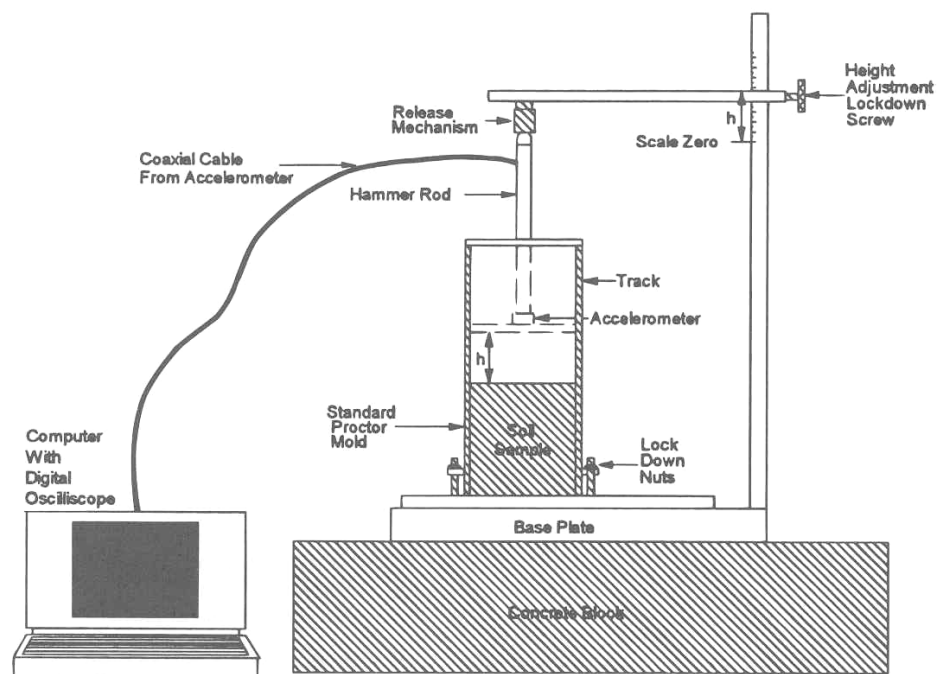


Figure 3.1 Equipment set up for the ATM device (Drumm et al. 1996)

Expressions for the modulus and deviator stress as a function of the measured acceleration during impact were developed using a simple theoretical model by Drumm et. al. (1996). They evaluated the resilient moduli from the new alternative test method for 14 soils from Tennessee and their values compared reasonably with the results from standard repeated load triaxial tests (Fig. 3.2). They also showed that the soils with low and high moduli

were consistently distinguished by the alternative method and the estimates of resilient modulus were considered satisfactory for most pavement design applications. The alternative method developed by Drumm et. al. (1996) was simple and advantageous to use in a production environment favoured by the familiarity of the Proctor test and the limited data collection requirements.

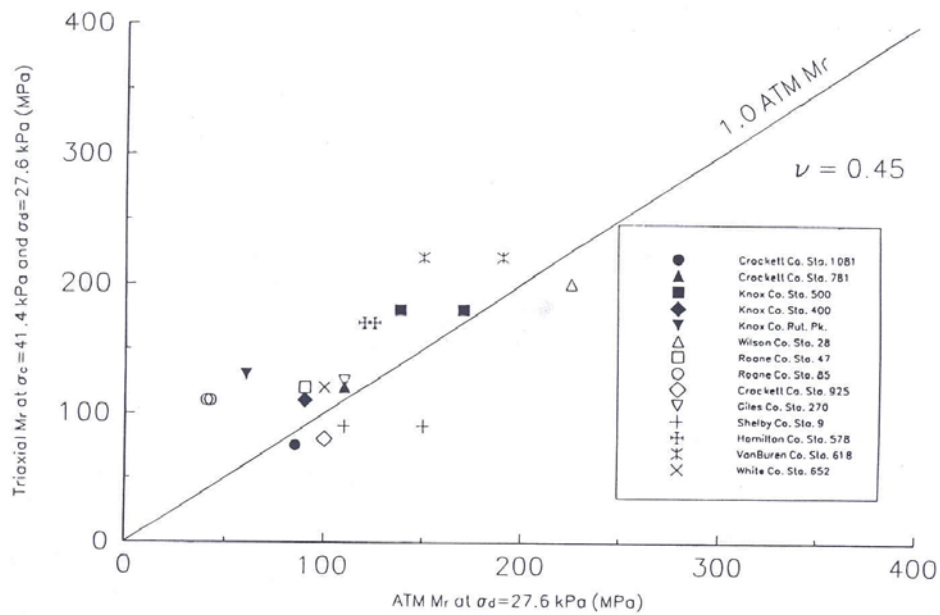


Figure 3.2 Comparison of cyclic triaxial and ATM resilient modulus test results (Drumm et al. 1996)

Kim et. al. (2001a,b) have developed an alternative resilient moduli (M_R) testing technique which is simple and reliable, considering the difficulties, complexities and prohibitive costs and time involved in performing the cyclic M_R testing. They proposed static triaxial tests as an alternative considering the effects of loading frequency, mean effective stress, number of loading cycles, and maximum particle sizes. Comparison of results with resonant column –torsional shear stress was also performed on seven subgrade samples (nonplastic sandy soils, plasticity index less than 5%, average CBR value 21) from several pavement projects.

Kim *et al.* (2001a,b) carried out loading, unloading and reloading stages of the static triaxial test, and the secant modulus was calculated from the slope of lines connecting the reversal origin to the reloading curve (E_r) or unloading curves (E_u) as shown in Fig. 3.3. It was found that the mean effective stress during the reloading stage $[(3\sigma_c + \sigma_{d,r})/3]$ of the static triaxial test was equivalent to those in the M_R test $[(3\sigma_c + \sigma_{d,M_R})/3]$ with a given seating pressure. The stiffness therefore was determined from the reloading curve of the static triaxial test with the same seating load as the standard M_R testing method.

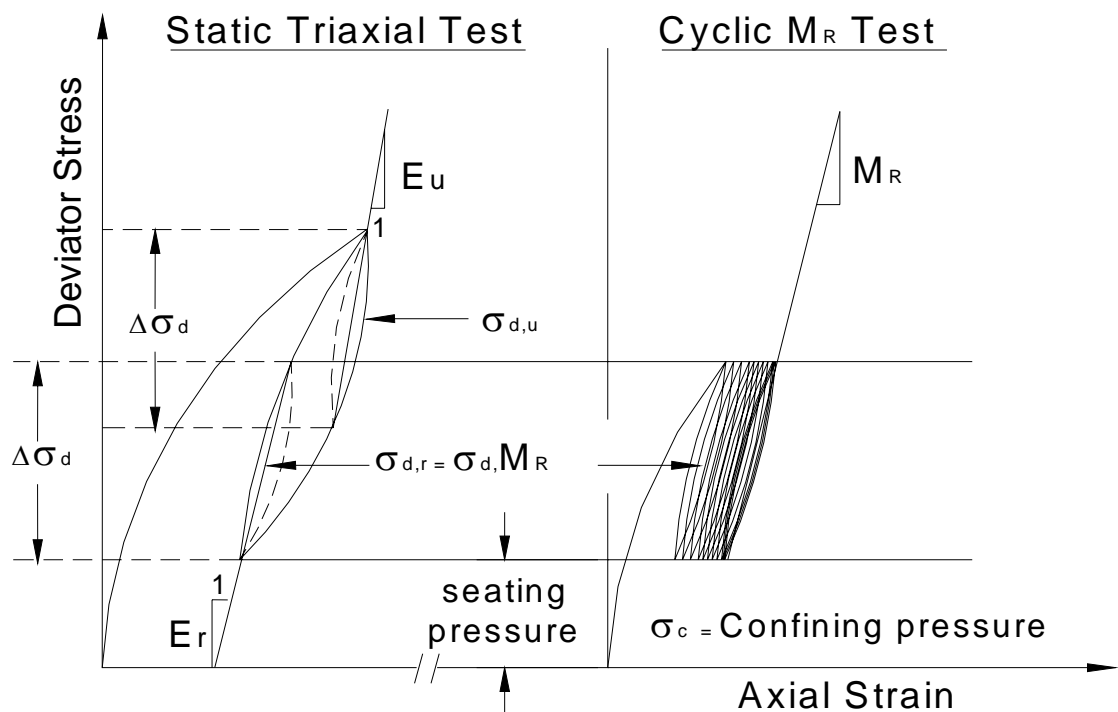


Figure 3.3 Comparison of mean effective stresses during static triaxial and M_R tests (Kim *et al.* 2001a)

Fig. 3.4 shows a typical comparison of this alternate method (Kim *et al.* 2001a,b) with the standard M_R test, for a non-plastic subgrade type SG-6, which was in good agreement. To evaluate the reliability of applying modulus values, a confidence level was evaluated under working stress conditions. As shown in Fig. 3.5, the 95% confidence interval of moduli obtained from the proposed method was $\pm 3.59\%$, and the moduli determined from the

proposed method were about 9% larger on average than those obtained from the standard M_R test. Considering the findings of Kim *et al.* (2001 and b), a similar approach was adopted in the current research to find the resilient material properties.

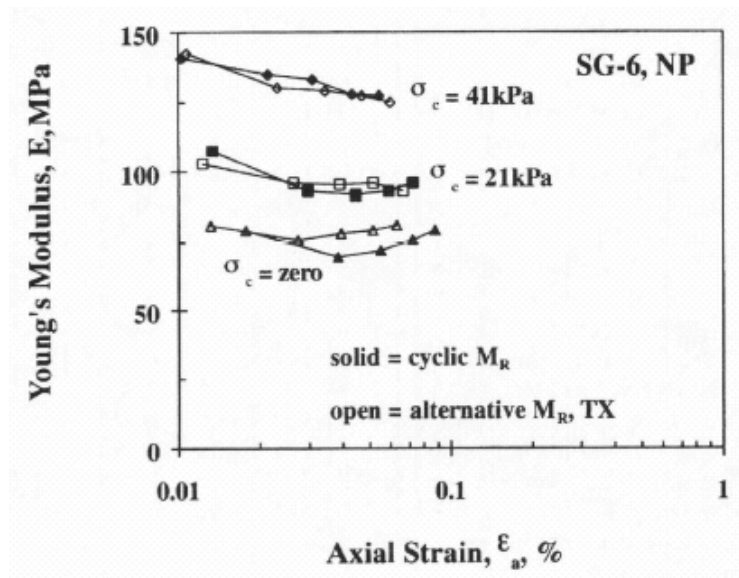


Figure 3.4 Comparison of M_R values with alternative method (Kim *et al.* 2001a)

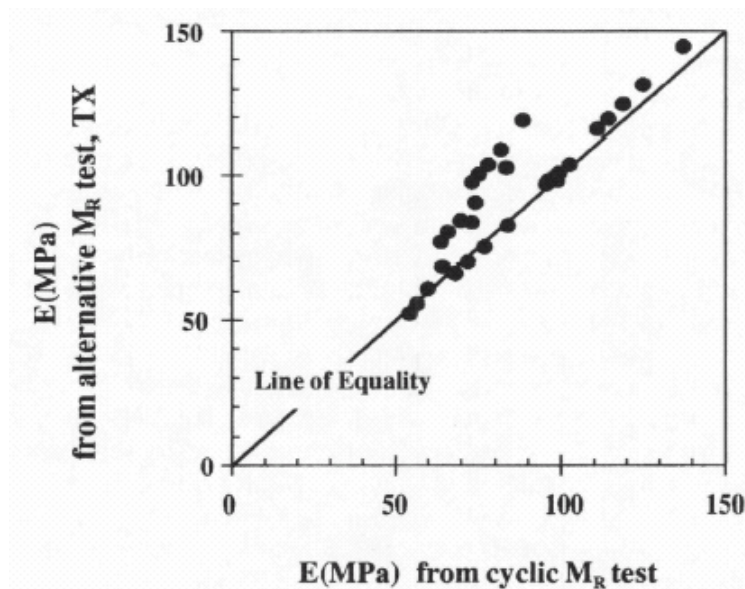


Figure 3.5 Evaluation of reliability of moduli determined by the alternative method (Kim *et al.* 2001a)

Okada and Ghataora (2002) have developed a quick and accurate method for measuring the stiffness of railway subgrades. A cyclic penetration test was introduced using the California Bearing Ratio (CBR) test mould (Fig. 3.6). A finite element analysis was carried out and cyclic stress distribution in the CBR mould was calculated.

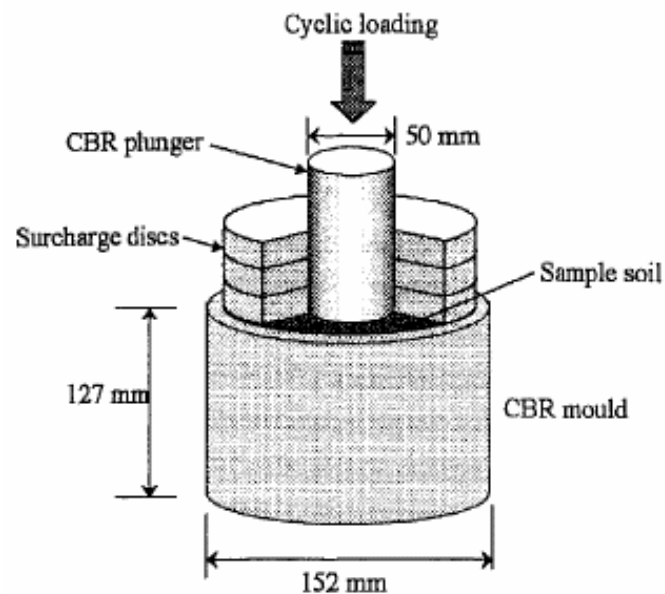


Figure 3.6 Cyclic penetration test apparatus (Okada and Ghataora 2002)

A plastic modulus M_p was defined using the cyclic stresses, which in turn was used to calculate the cumulative plastic deformation (for soil in a CBR mould). These results were then correlated to cumulative settlement of subgrade using the Talbot equation and a power model. The results were compared with measured settlements at actual railway sites by Heath et. al. (1972) and reported to be in good agreement.

The main advantage of this method is that it can be easily used to design ballast depth by limiting allowable subgrade settlement. A reliable indicator for the maximum acceptable soil moisture content defined as 'threshold moisture content' was also determined. The determination of the relationship between the penetration of plunger and moisture content

was by normalising both values, for London clay, Oxford clay and building sand. The normalised moisture content is the ratio of moisture content to optimum moisture content and the normalised penetration is the ratio of penetration to penetration at optimum moisture content. There was a sudden increase in penetration at certain levels of normalised moisture content of 1.1 to 1.4 as illustrated in Fig. 3.7. This sudden changing value was termed the threshold moisture content and it was found that wet subgrades exceeding this threshold value potentially failed prematurely. The significance of maintaining adequate drainage in subgrade to maintain its stiffness is therefore apparent as the plastic deformation of soil significantly increases especially when the soil is nearly saturated.

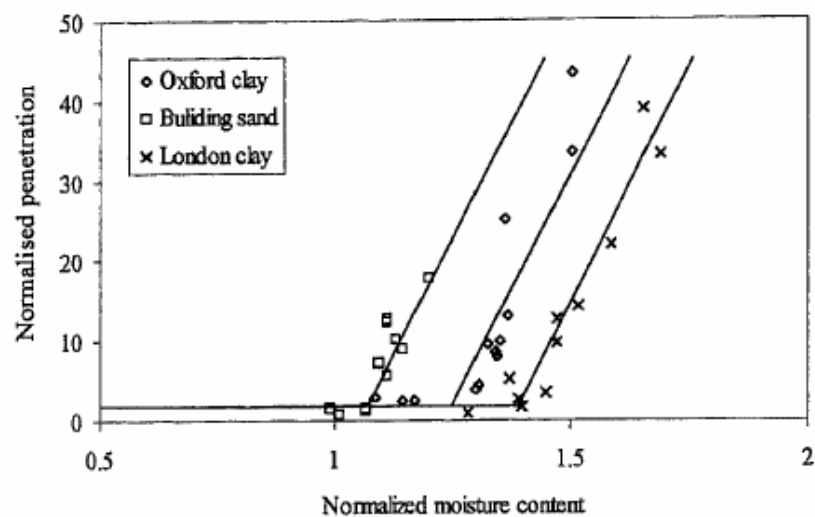


Figure 3.7 Relationship between moisture content and plunger pressure (Okada and Ghataora 2002)

With the advent of modern computerised numerical models, the analysis procedures have become more effective and reliable at incorporating complexities in geometry, boundary conditions and material properties. Dahlberg (2001) has summarised mathematical models currently available in the literature, emphasising that track settlement is mostly considered

as a function of loading cycles and/or a function of the magnitude of the loading, but very little is available in the literature dealing with the material properties of track substructure.

The major reasons for current design methodologies not addressing the permanent deformation of substructure are:

- expensive, tedious and time-consuming experiments;
- implicit consideration of subgrade deformations as insignificant; and
- assumptions of the distress caused by loading as highly dependent on the resilient properties rather than plastic properties of subgrade.

However, present trends focus on maintaining the level of the geometry for the top layers of the railway track, sub-ballast and capping layers within very strict tolerance levels. As permanent deformation of these layers is the major contributing factor to the geometry tolerance issues, it would be prudent to include the calculation of deformation of such layers during the design stage itself. This thesis therefore aims at developing an inexpensive method of determining both the recoverable and irrecoverable moduli of the capping layer.

This Chapter first states the aim of the experiments and the methods of testing; second it outlines the selection of material for testing and examination of its properties followed by the experimental setup, typical experimental results and discussions. Dimensional analysis and ternary plots are then detailed for further analysis of the experimental results. The relevant data of Chapter 3 are exhibited in detail in Appendices A.1 – A.7.

APPENDIX A.1	Basic properties of the capping layer material
APPENDIX A.2	Density and saturation calculations- Semi Confined Test (SCT) samples
APPENDIX A.3	SCT experimental data sheets

APPENDIX A.4	Stiffness and penetrated depth against moisture, penetration rate and number of cycles in SCT
APPENDIX A.5	Dimensional analysis data sheets
APPENDIX A.6	Coefficients of the orthogonal polynomials
APPENDIX A.7	Ternary plot calculations

3.2 Semi-Confined Cylinder Test (SCT)

3.2.1 Aim of Testing

In-situ tests normally produce measurable structural responses (for example, load-settlement curves) and the material properties of the constituent layers are determined via backcalculation of layered subgrades. However limitations are prominent in in-situ testing as a large number of un-controllable environmental variables (moisture, temperature, etc.) usually influence the results. Laboratory tests, on the other hand, determine actual parameters without influences from other material layers. The laboratory studies for evaluation of permanent deformation are less advanced than for resilient deformations. The existing test procedures for permanent deformation evaluation are relatively complex and laborious. As such, further development on methods assessing permanent deformation and correlation of resilient behaviour to simpler tests is required.

The main aim of this thesis is to develop an economical method to evaluate the stress-strain relationship of capping layer which would have the potential to be used as a routine assessment approach for the characterisation of granular soils comprising the rail track substructure.

Mathematical models of the behaviour of soils have been developed since late 1940's as discussed in Section 2.4. These methods show that qualitative agreements can be found

with experimental results even by means of simple elasto-plastic models. As such in this research a simple strain controlled penetration testing of soil specimens contained in a rigid cylinder is proposed. The material properties are then predicted via a finite element simulation based backcalculation technique.

3.2.2 Design of experiments

It was decided to perform an extensive series of tests on a benchmark material in order to obtain a complete data base with which to compare the modelling predictions. In developing an economical method, it was also decided to use the typical CBR mould as the apparatus for the testing. The CBR mould is capable of approximating the drained conditions observed in-situ.

Two major parameters that affect the behaviour of railway substructure were considered in the design of experiments. They were the moisture ingress and the train speeds.

Furthermore all categories of test specimens were subjected to two loading sequences; 1) monotonic loading and 2) cyclic loading. In the monotonic tests the penetration was continuously increased to a substantive level at a constant rate. In the cyclic tests the displacement was applied at a constant rate in a sequence of loading, unloading and reloading at pre-decided penetration levels. Fig. 3.8 provides a sketch of these two penetration sequences. It also shows possible load-penetration profiles that can be expected of this form of penetration sequences. In both cases only the vertical penetration was considered.

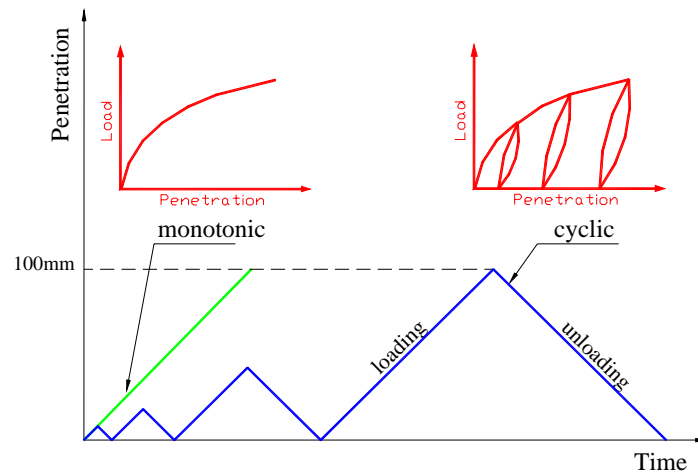


Figure 3.8 Monotonic and cyclic loading sequences

Moisture States

In practice, the compaction of the railway subgrade is carried out at Optimum Moisture Content (OMC). Therefore to assess the effect of the moisture ingress on the behaviour of the capping layer; OMC (moist), dry and saturated (wet) were considered in the experiments. All specimens were made first by compacting at OMC in line with the engineering standard for “modified compaction”. In simulating the three states, the samples were tested as-prepared (OMC or moist state) or tested after modifying the level of moisture in them. The moisture levels were modified by soaking for four days (96hrs.) or after drying in an oven at 105⁰C for one day (24hrs.), to examine the effect of saturated (wet) and dry conditions respectively. For illustrations in the diagrams, these three conditions OMC, saturated and dry are referred to as M, S and D respectively.

Loading Rates

The effect of train speed has an influence on the behaviour of the substructure. The effect of train speeds are generally investigated in terms of resulting dynamic vertical loads on tracks (Zhang 2000). There are three main wave types caused by the vibrations in soil through which each wave propagates; Surface or Rayleigh waves, P-waves or compression

waves, and S-waves or shear waves. The soil particles will start to move locally when these earthborne waves pass through the soil medium. Usually these particle velocities are measured, analysed or reported as vertical, horizontal longitudinal, horizontal traverse, or the resultant of all three motions. Most often (although not always), the vibrations along the ground are greatest in the vertical direction and usually a Peak Vertical Particle Velocity (PVPV) is reported for earthborne vibrations (Hendriks 2002).

The vibration levels caused by trains will vary depending on the speeds, loads, condition of track and the amount of ballast used to support the track. Fig. 3.9 shows PVPV's caused by the passage of trains, measured at 5m from the train where the PVPV of 7mm/s was observed which diminishes with increasing distance from the train to about 0.25mm/s at about 90m (Hendriks 2002). It also shows some risk levels suggested in literature for various types of buildings.

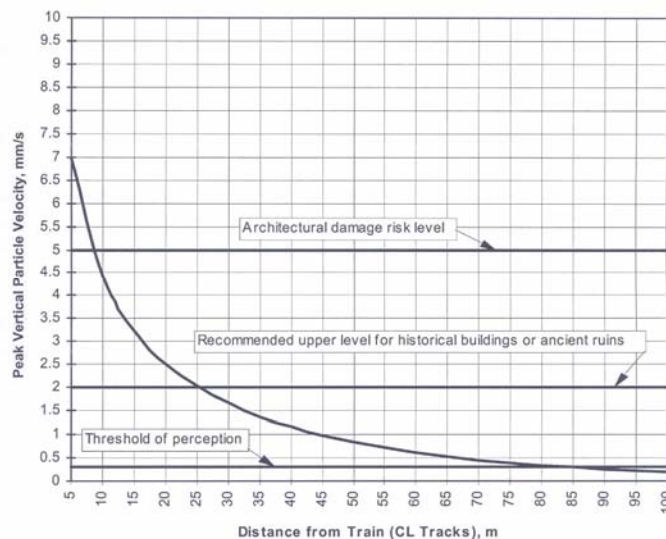


Figure 3.9 Maximum train vibration levels reported at Sacramento, CA, USA (Hendriks 2002)

The peak particle velocities for Japanese and Swedish trains were reported by Dowding (2000). For Japanese trains travelling slower than the wave propagation velocity, the peak

particle velocities recorded were 4mm/s and 7mm/s at a distance of 25m from the train in soft ground and stiff ground respectively. For Swedish trains travelling at greater speeds than the wave propagation velocity the recorded velocities were 200mm/s at a distance of 3m and 17mm/s at a distance of 9m from the train (Dowding 2000).

Hall (2003) too has tested train induced vibrations caused by a trains travelling at various speeds gradually increasing from 10, 70, 120, 140, 160, 180 to 200km/hr at high-speed project of Banverket, Sweden. Fig. 3.10 shows the PVPV's caused by a train travelling at a speed of 142km/hr. It can be seen that the reported PVPV's were between 2.5mm/s to 18mm/s showing a very wide velocity range of the soil particles.

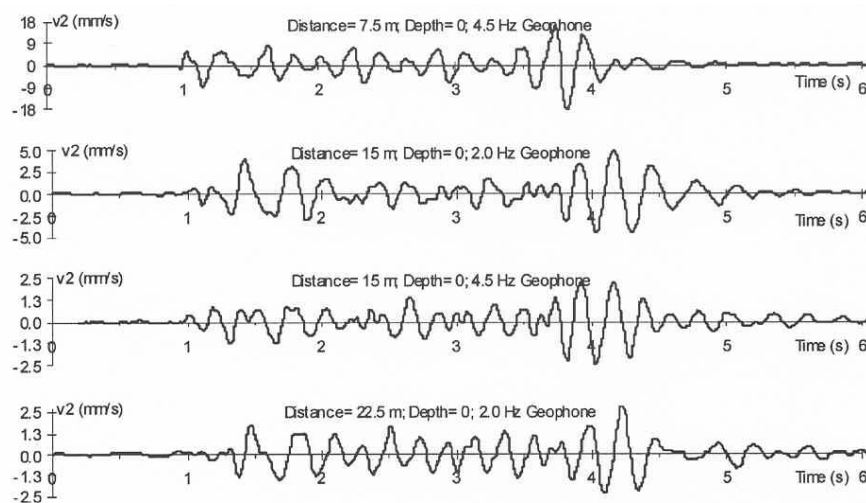


Figure 3.10 Vertical particle velocity response reported at high-speed project of Banverket, Sweden (Hall 2003)

As per the above discussion, by considering the wide range of the PVPV's (2.5-18.0mm/s) caused by the train induced wave propagations and the available test equipment limitations encountered, it was decided to carry out tests for five penetration rates 2.5, 5.0, 10.0, 15.0 and 20mm/min. This range was considered representative enough as usually the tests to measure stress-strain properties of a soil in drained conditions are carried out at low rates.

The wave propagation velocities in all types of soils (granular and cohesive) were influenced by their void ratio and the mean effective confining stress they were subjected to. Saturation also influences the wave propagation velocities. In partially saturated (10-50% saturated) fine granular soils (silty sands) the capillary pressures have increased the shear modulus by 50-100% increasing the wave propagation capacity of the soil (Gazetas 1991)

Thus, thirty (30) experiments were carried out for the above conditions stipulated; two (02) loading sequences \times three (03) moisture states \times five (05) penetration rates.

3.3 Material Selection

The benchmark material selected for the study is described as MRD Type 2.4 Unbound soil, obtained from the CSR Quarry at Nerimbera, Central Queensland, Australia. The material must meet the requirements of having a minimum soaked CBR of 35 at 100% standard compaction effort and a maximum Plasticity Index (PI) of 12 and maximum Weighted PI of 360 (Main Roads MRS11.05 1999). The Department of Main Roads, Queensland, Australia, uses this material as a base or sub-base layer in road pavements. Queensland Rail (QR) sometimes uses this material as a capping layer in railway substructure. As such, investigation of the behaviour of this material is expected to benefit both the road pavements and the railway subgrades designs.

Fig. 3.11 illustrates the particle size distribution (PSD) envelope of the material used in the laboratory testing. From the PSD curve we could infer that it is a well-graded material; therefore, care was taken to avoid segregation of particles during placement and testing.

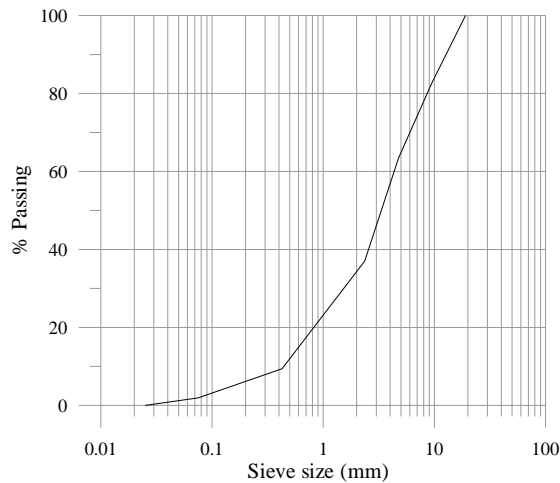


Figure 3.11 Particle size distribution of Type 2.4 Unbound Material

Table 3.1 presents the basic properties of the material selected. The material showed a permeability of 10^{-2} m/sec, which is close to permeability of very fine sands, silts and clay-silt laminate (Craig 1997). From the properties listed, the material can be classified as a *well graded mixture of very sandy gravel with traces of non-plastic fine with a medium permeability*. The corresponding property evaluations are located in Appendix A.1.

Table 3.1 Properties of Type 2.4 Unbound Material

Material property	Measured Value	Reference
Specific gravity from multi-pycnometer test	2.75	(Quantachrome Corporation 1996)
Linear shrinkage	2.4%	(AS 1289.3.4.1 1995)
Liquid limit from cone penetrometer method	20%	(AS 1289.3.9.1. 2002)
Maximum dry density from modified Proctor compaction test (γ_{dmax}) t/m ³	2.31	(AS 1289.5.2.1 2003)
Optimum moisture content at maximum dry density (w_{max})	5.9%	(AS 1289.5.2.1 2003)
Coefficient of uniformity ($C_U = D_{30}^2 / D_{60}D_{10} >4$)	7	(Craig 1997)
Coefficient of curvature ($1 < C_z = D_{30}^2 / D_{60}D_{10} <3$)	1.8	(Craig 1997)
96hrs Soaked California Bearing Ratio (CBR) using modified compactive effort	110	(AS 1289.6.6.1 1998)
Permeability (K) at 20°C of a modified compacted sample m/sec	1.1×10^{-2}	(AS 1289.6.7.2 2001)

Note:

D_{60} , D_{30} , and D_{10} are the particle size such that 60%, 30% and 10% of the particles are finer than that size respectively.

3.4 Experimental Setup

The CBR mould (152mm diameter, 177.5mm high) was used to prevent overall lateral bulging of the test specimen due to the development of relatively high confining pressures generated by the vertical penetrations. Vertical bulging (Fig. 3.12) through the unconfined top surface of the specimen was, however, possible. Therefore, this test is regarded as semi or partially confined. The vertical penetration was imposed by a servo-hydraulic loading system with a capacity of 500kN fitted to a rigid portal frame, via a rigid solid steel cylinder of length 200mm and diameter 50mm. This provided a solid barrier to the disturbed failed material, not allowing it to fall back into the indentation formed during the process of penetration. The specimen was centred under the load cell and load-penetration behaviour was recorded by the data-acquisition system. The tests were stopped either when the penetration exceeded 100mm or when the load reached the 500kN capacity of the system (equivalent to $255 \times 10^3 \text{ kN/m}^2$).



Figure 3.12 Experimental Setup

3.4.1 Test Procedure

- Step 1. The material was air dried and sieved through a 19mm sieve to remove any oversize particles.
- Step 2. The material was homogenised with the required amount of water at the OMC and thoroughly mixed and cured for a minimum of 2hrs as its liquid limit was low (Table 3.1).
- Step 3. The material was then compacted in a greased standard CBR mould in five layers, each of about 35 mm thick subjected to 56 blows with the 4.9kg Proctor hammer falling a distance of 450mm.
- Step 4. After compaction, the excess material protruding into the collar was removed with a blade and the top surface was levelled.
- Step 5. The sample weight was noted at OMC.
- Step 6. To obtain a dry sample, the sample compacted at OMC was oven dried at a temperature of 105⁰C for 24hrs. For a saturated sample, the sample, compacted at OMC, was soaked for 96hrs in water.
- Step 7. For dry or saturated samples the weight of the sample was noted again prior to testing.
- Step 8. The sample was then centred under the load cell of the hydro-servo machine.
- Step 9. The load was applied at the required loading sequence and the penetration rate.
- Step 10. The load-penetration data were recorded.
- Step 11. The tested sample was removed from the mould and void ratio and moisture content were determined.

3.4.2 Testing Program

A total of 30 specimens were tested. Monotonic tests were conducted typically within 10-40 minutes depending on penetration rates. Cyclic tests consisted of 10 cycles minimum and took 20-80 minutes. Table 3.2 illustrates the test program employed. Each specimen was provided with a unique tag of four characters. The first character represents the loading type (C for cyclic; M for monotonic). The second character represents the moisture level (M/S/D as explained before). The third and fourth digits represent the approximate loading rate in mm/minute for 2.5mm/min, and the actual rates used otherwise. That is 02 for 2.5mm/min, 05 for 5.0mm/min, 10 for 10.0mm/min, 15 for 15.0mm/min and 20 for 20.0mm/min.

Table 3.2 Laboratory testing program

Specimen number		Penetration rate (mm/min)	Moisture content	
Monotonic	Cyclic			
MM02	CM02	2.5	Optimum moisture content	M
MM05	CM05	5		
MM10	CM10	10		
MM15	CM15	15		
MM20	CM20	20		
MS02	CS02	2.5	96hrs. saturated sample	S
MS05	CS05	5		
MS10	CS10	10		
MS15	CS15	15		
MS20	CS20	20		
MD02	CD02	2.5	24hrs. oven dried sample at 105 ⁰ C	D
MD05	CD05	5		
MD10	CD10	10		
MD15	CD15	15		
MD20	CD20	20		

3.4.3 Density and Moisture Contents of the Specimens Tested

Table 3.3 shows the moisture content and the density of all the specimens tested. The difference between the moisture contents of the OMC and saturated specimens was found to be about 1.0%. The dry specimens showed some amount of moisture contained in them though they were oven dried for 24hrs at 105⁰C. The densities of the samples did not vary much although their moisture levels were different. The degree of saturation of each specimen was calculated and presented in Appendix A.2. It can be concluded that the load bearing capacity has reduced with the increase in moisture as the density of the material has been reduced.

Table 3.3 Specimen properties

Monotonic Tests (MT)			Cyclic Tests (CT)			Average of MT & CT		
Specimen Number	Density (kg/m ³)	Moisture content (%)	Specimen Number	Density (kg/m ³)	Moisture content (%)	Density (kg/m ³)	Moisture content (%)	
MM02	2464	5.93	CM02	2394	5.86	2429	5.90	M
MM05	2372	5.66	CM05	2396	5.7	2384	5.68	
MM10	2475	5.74	CM10	2502	5.69	2489	5.72	
MM15	2461	5.53	CM15	2471	5.71	2466	5.62	
MM20	2459	5.46	CM20	2477	5.74	2468	5.60	
Average	2446	5.66	Average	2448	5.74	2447	5.70	
MS02	2375	7.03	CS02	2405	6.71	2390	6.87	S
MS05	2366	7.3	CS05	2411	6.31	2389	6.81	
MS10	2475	7.16	CS10	2496	6.51	2486	6.84	
MS15	2486	6.62	CS15	2471	7.27	2479	6.95	
MS20	2489	6.79	CS20	2411	6.82	2450	6.81	
Average	2438	6.98	Average	2439	6.72	2439	6.85	
MD02	2365	0.45	CD02	2332	0.5	2349	0.48	D
MD05	2275	0.75	CD05	2353	0.51	2314	0.63	
MD10	2367	1.63	CD10	2343	0.68	2355	1.16	
MD15	2359	1.14	CD15	2381	1.32	2370	1.23	
MD20	2357	1.15	CD20	2276	1.33	2317	1.24	
Average	2345	1.02	Average	2337	0.87	2341	0.95	

3.5 Results of Semi-Confined Cylinder Test (SCT)

This section presents the results of the SCT with the discussion highlighting observed behaviour and possible trends. The effect of moisture content and the rate of penetration on the behaviour of specimens are also discussed. Dimensional analysis is used as a tool to analyse the effect of penetration rate. Finally a ternary plot is presented to illustrate the relationship between the density of the sample, penetration rate and the moisture content. The corresponding experimental data sheets are located in Appendix A.3.

3.5.1 Behaviour of Material under SCT Setup

A highly non-linear behaviour with respect to loads was observed in the displacement-controlled tests carried out in the rigid CBR cylinders. The trend indicated in Fig. 3.13 therefore gives the entire picture of the data recorded. Four types of behavioural response were observed in each experiment, namely; hardening, stabilising, softening and remoulding. The initial response of hardening effect is typical of most elasto-plastic materials. This response changed rapidly with the increase in initial confinement stresses generated by the vertical stresses. Following the hardening phase, subsequent increase in penetration of the specimens exhibited a stabilising phase with little or no increase in resistance to penetration. Subsequently a softening in resistance to penetration occurs. With further increase in penetration the specimen then regains stiffness (K') and behaves like a virgin soil, although it does not become as stiff as it was initially (K_0). This range was defined as the “remoulding range” in Fig. 3.13. The specimen exhibited these four phases of behaviour at several stages (*Stage I, Stage II,...*) throughout the penetration path. As illustrated in the inset of Fig. 3.13, the dried samples showed more dominant patterns of the qualitative response described above than the OMC or saturated samples. It can also be

seen that the load carrying capacity has greatly reduced from dry to saturated states as shown in the inset of Fig. 3.13. This can be best described by taking into consideration the adhesive bonding between each point of individual contacts between the soil particles.

Every soil carries an electric charge on its mineral surface and attracts molecules of water or other impurities. As water is introduced the ions hydrate and are less strongly attached to the mineral surfaces (Lambe and Whitman 1979). Thus, in the oven-dried dry samples, the ions are not completely hydrated allowing the actual mineral surfaces to become close together making a strong bond with each other. In the OMC and saturated samples the water has hydrated the ions reducing the effect of the strong bonds between the mineral particles. Thus, the shear resistance has dropped in OMC and saturated samples as water is introduced showing that water acts as a lubricant making the samples weaker.

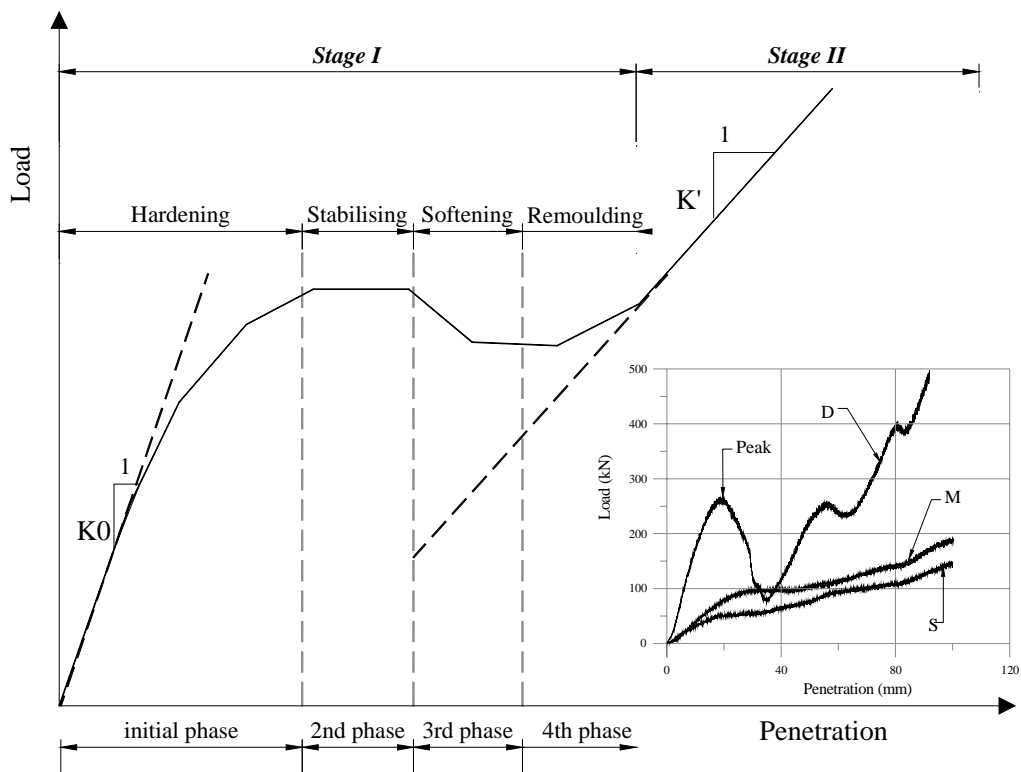


Figure 3.13 Typical load-penetration behaviour in a test

For the initially generated confining pressures, the softening phase is associated with a peak as shown in the dry state of the inset in Fig. 3.13. The lower the confining pressure the more dilatant is the behaviour after the peak. The occurrence of a peak is always associated with the development of a fracture plane in the specimen. For very high confining pressures, hardening starts from the beginning of the shearing phase. Also, for dry specimens it is apparent that the stiffness is lower than the initial stiffness appropriate to tests at much lower initial confining pressures. However, the OMC and saturated specimens show a more “ductile” behaviour compared to the brittle nature of the dry specimens.

The above phenomena can be further explained using the dilation and collapse mechanisms theorised by Bowles (1979). According to the theory the dense soils tend to dilate or expand while the loose soils tend to collapse or densify under shear. In a dense state, dilation occurs with the net effect being an increase in volume (+V) as the particles are forced up, over and around adjacent and confining grains. In a loose state, the net effect is a decrease in volume (-V) as the particles are moved into the voids. Fig. 3.14 illustrates this phenomenon.

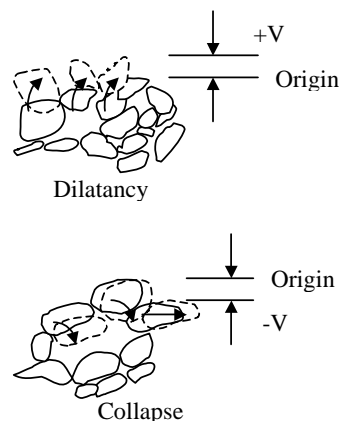


Figure 3.14 Dilatancy and Collapsing effects under shear of cohesionless soils (Bowles 1979)

Lambe and Whitman (1979) discussed similar patterns observed in granular materials in dry conditions. The initial phase of the load-penetration curve shows interlocking of particles with increase in stress, but the second phase shows the onset of a reverse curvature. This appears to be due to yielding causing fracturing of individual particles, which permits large relative motion of individual particles. The fracturing of particles may even cause an incremental momentary collapse range (3rd phase in each stage) and further increase in stress enhances tighter packing of the new and remaining particles making the specimen stiffer. Remoulding phenomenon is also described by Bowles (1979). It is stated that particulate material like soil fails primarily due to rolling and slipping of grains and defines failure as a considerable alteration or state change in soil structure (or remoulding).

3.5.2 Monotonic and Cyclic Loading Behaviour

Figs. 3.15 -3.19 show the results of six specimens under each category of the loading program. In each pair one specimen was monotonically loaded while the other was subjected to many cycles of loading-unloading-reloading.

(i) Envelope response

The saturated specimens subjected to cyclic load exhibited higher resistance to penetration than their monotonic counterparts at 2.5, 5 and 10mm/min penetration rates. At 15 and 20mm/min penetration rates both the monotonic and cyclic load tests exhibited almost equal resistance.

Except for the 2.5mm/min penetration rate OMC specimen, all other OMC specimens subjected to cyclic loads exhibited lower or almost equal envelopes of resistance to penetration than that of monotonic loading.

Dry specimens showed varying levels of envelopes of resistance due to cyclic and monotonic penetrations without any systematic patterns.

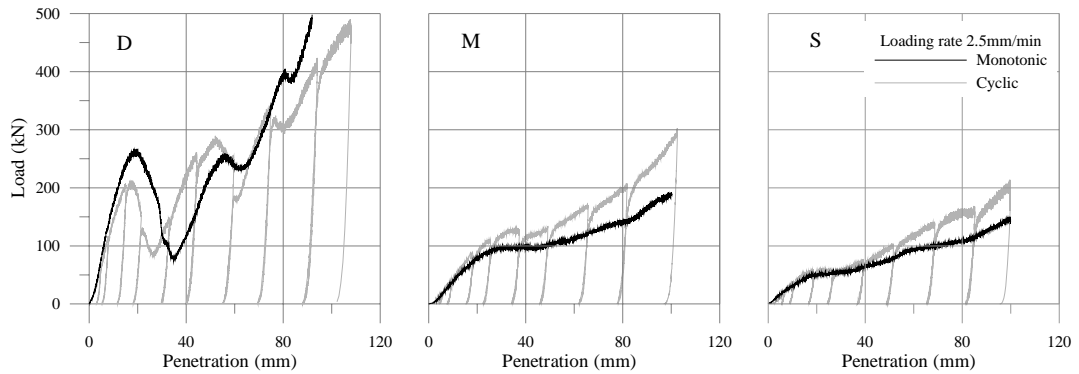


Figure 3.15 Behaviour during reloading at 2.5mm/min loading rate

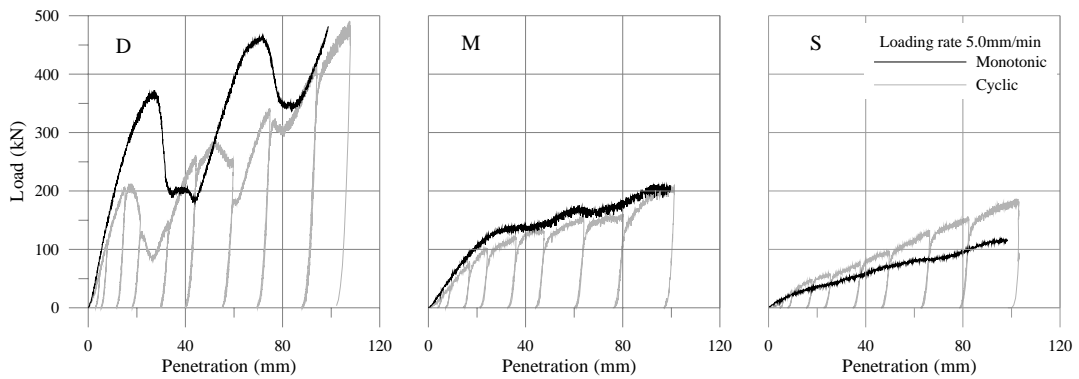


Figure 3.16 Behaviour during reloading at 5.0mm/min penetration rate

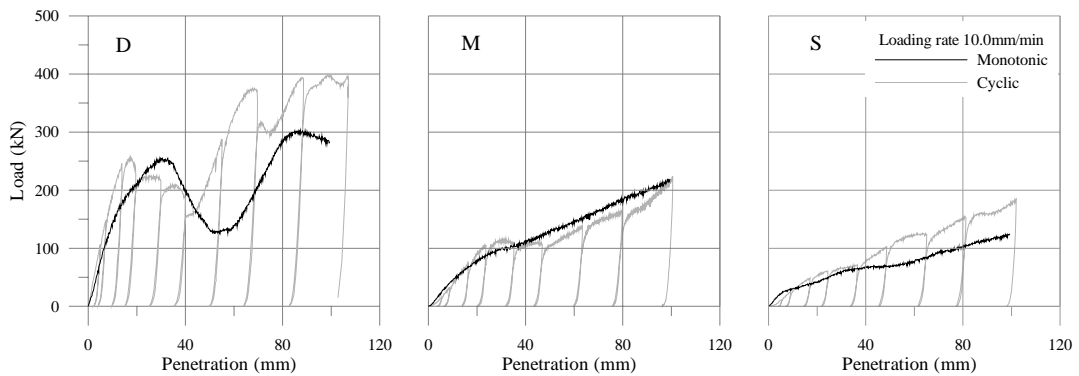


Figure 3.17 Behaviour during reloading at 10.0mm/min penetration rate

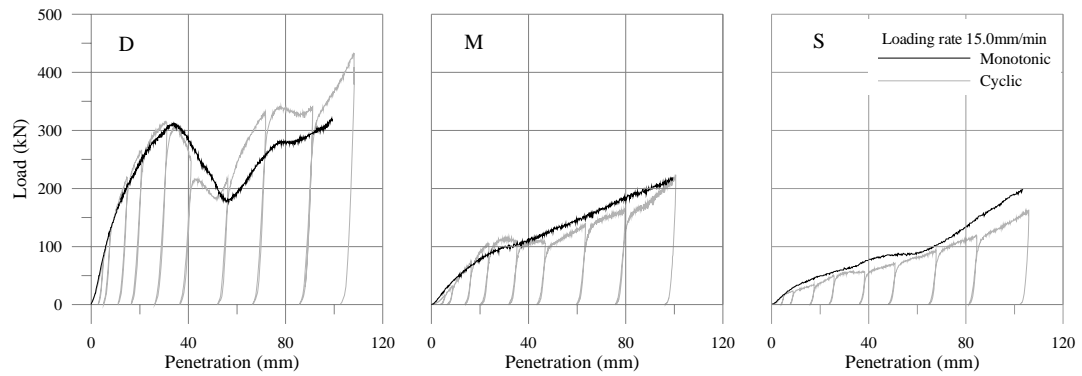


Figure 3.18 Behaviour during reloading at 15.0mm/min penetration rate

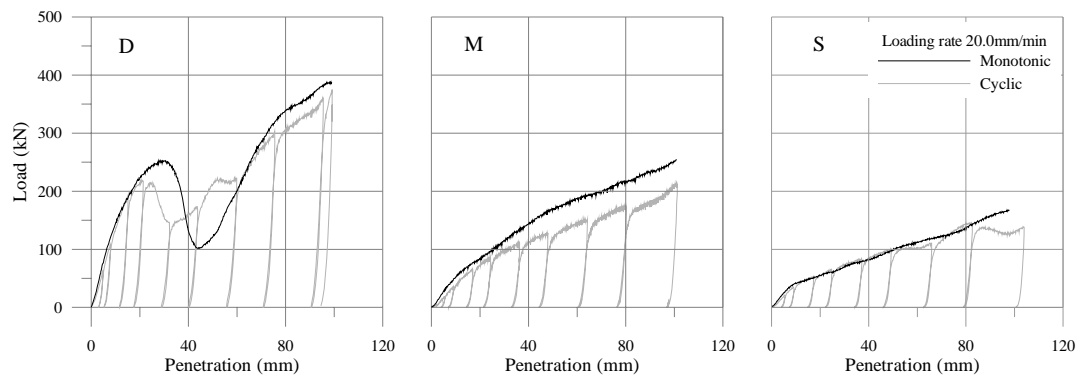


Figure 3.19 Behaviour during reloading at 20.0mm/min penetration rate

In summary, with the limited number of specimens tested (30 samples) in each category, it can be stated that the envelope response of the load-penetration curves could be arranged regardless of the type of loading application (cyclic/monotonic). This statement simplifies evaluation of the material constitutive relations from the monotonic penetration tests that are relatively economical to perform.

It is also evident from the experiments (Fig. 3.20) that three distinctive groups can be formed according to the level of moisture in the specimens irrespective of monotonic/cyclic load application or penetration rate. The variation caused due to type of loading, penetration rate as well as subjective deviations in density, moisture contents, and compaction while making each of the specimens are all captured in the three data groups

for dry, OMC and saturated states. The variation in all behavioural patterns can be easily accommodated by defining lower and upper bounds for each of these groups. Such simplification is reasonable in geotechnical evaluations as properties of soil directly depend on the soil conditions (initial density, degree of saturation, state of stress, initial grain size and type of restraints they are subjected to) which vary spatially even within relatively small distances in the field.

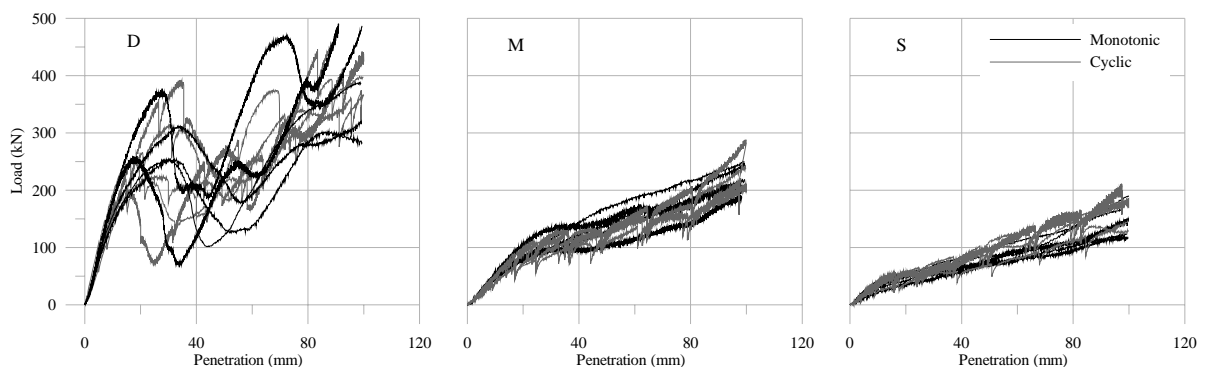


Figure 3.20 Behaviour during monotonic and cyclic loading at all penetration rates

(ii) Unloading-reloading response

The unloading-reloading behaviour is illustrated in Fig. 3.21. The stiffness at initial and various reloading paths are calculated using tangents drawn considering the respective linear parts as shown in Fig. 3.21. The initial loading path OA with initial stiffness K_1 is found to be significantly lower than the reloading path BC with the first reloading stiffness K_2 . Further the material showed an elasto-plastic behaviour when load was removed, very little deformation being recovered by elastic rebound as illustrated in Fig. 3.21. Irrespective of the number of loading and reloading cycles, the specimen behaves like a virgin soil during each re-loading cycle.

Moreover the slope of unloading-reloading relationship is only marginally affected by the occurrence of plastic strains. Therefore the occurrence of unloading-reloading cycles of limited amplitude does not influence the behaviour of the material under further loading. At least as a first approximation the unloading-reloading cycles appear to be linear elastic. In brief it could be stated that under unloading-reloading cycles

- (i) the reloading stiffness exhibits sequential increase and
- (ii) significant plastic deformation accumulates.

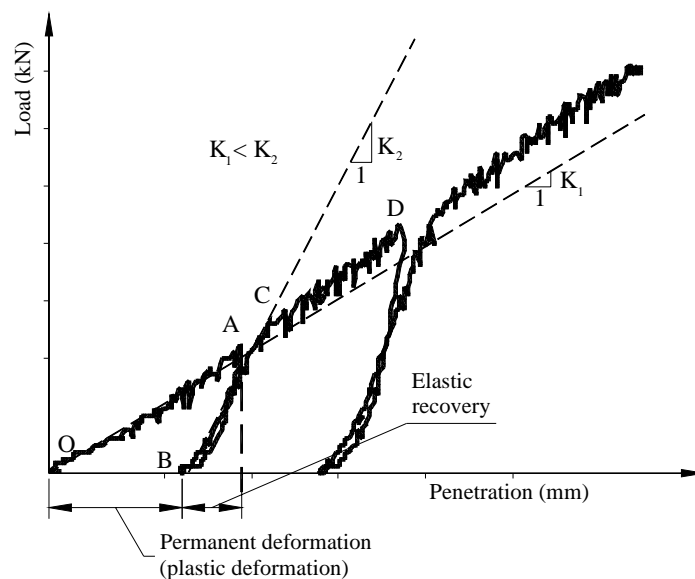


Figure 3.21 Typical unloading-reloading behaviour after the first loading

- (iii) Effect of number of load cycles

Fig. 3.22 further elaborates the behaviour explained in (ii) against number of loading cycles. The stiffness increases markedly between the initial loading cycle (K_1) and the first reloading cycle (K_2) as shown in Fig. 3.22. The dry samples showed very stiff behaviour compared to OMC and saturated samples. From K_2 onwards the dry samples showed a stiffness range of 28-70kN/mm at the lower bound. For OMC the lower bound range was 7-30kN/mm, while for saturated samples the range was 5-23kN/mm indicating almost similar behaviour to that of OMC but with a slight reduction in strength. The dry samples

showed a remarkable increase from OMC and saturated while the latter two projected an overlapping region. The relevant data sheets are located in Appendix A.4.

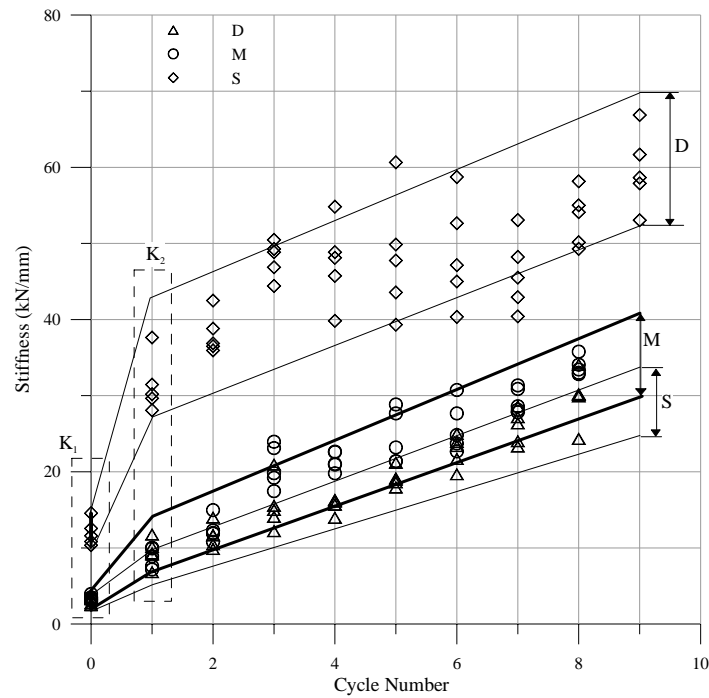


Figure 3.22 Stiffness during initial loading and reloading

In order to determine the effect of the number of load cycles to the predetermined permanent deformation (δ), the deformations were plotted against the cycle number (N) as shown in Fig. 3.23. It can be seen that there is a range in variation from lower penetration rates to higher rates. By considering all data points, irrespective of their rates, the best fit curves are found to be of the power form given by,

$$\begin{aligned} \ln(\delta) &= A \times \ln(N) + B \text{ or} \\ \delta &= c N^d \end{aligned} \quad (3.1)$$

where A , B , c and d are constants.

The three relationships obtained are given in Eqs. (3.2)-(3.4) for dry, OMC and saturated samples respectively together with their coefficient of determination R^2 values.

$$\begin{aligned} \ln(\delta) &= 1.48 \times \ln(N) + 0.98 \text{ or} \\ \delta &= 2.67 N^{1.48}, R^2 = 0.97 \end{aligned} \quad (3.2)$$

$$\begin{aligned} \ln(\delta) &= 1.44 \times \ln(N) + 1.23 \text{ or} \\ \delta &= 3.43 N^{1.44}, R^2 = 0.98 \end{aligned} \quad (3.3)$$

$$\begin{aligned} \ln(\delta) &= 1.40 \times \ln(X) + 1.33 \text{ or} \\ \delta &= 3.91 N^{1.41}, R^2 = 0.98 \end{aligned} \quad (3.4)$$

The dry samples showed least permanent deformations with the increasing cycle number while the saturated and OMC samples showed almost similar permanent deformations. Therefore it can be concluded that the moisture content should be the main consideration in any design together with the effect of load cycles.

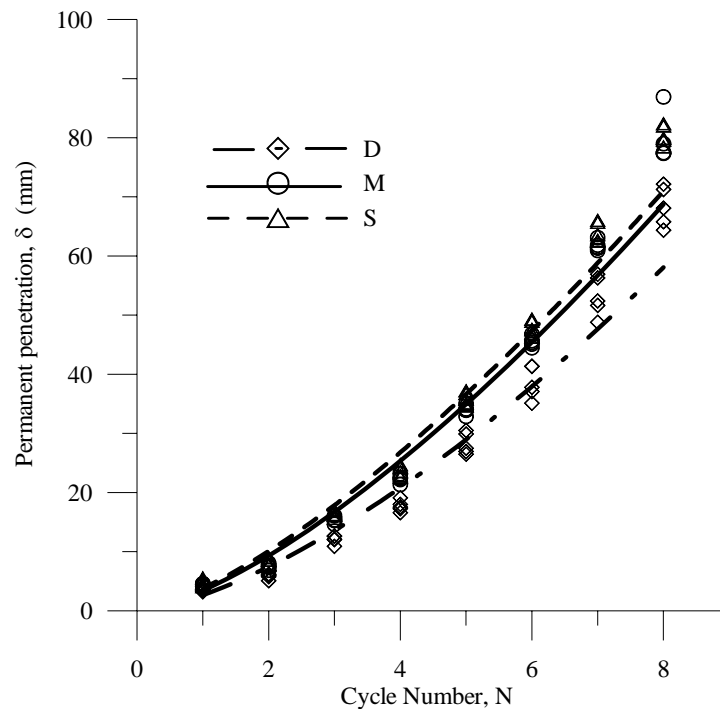


Figure 3.23 Penetration against cycle number

3.5.3 Effect of Moisture Content

In practice the natural phenomena of drying and wetting could lead to brittle and yielding types of failure in a cyclic manner causing differential settlements in the track subgrade.

This was very much evident in the respective experiments of dry, OMC and saturated

states as shown in Fig. 3.24. The brittle nature is predominant in dry state while OMC and saturated states showed some ductility in their responses.

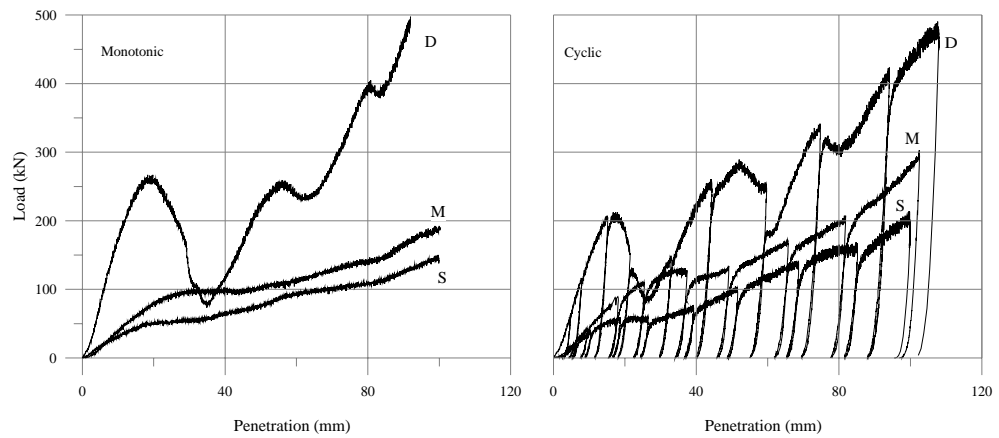


Figure 3.24 Effect of moisture content (dry specimens)

The effect of moisture on the stiffness of specimens was determined by first calculating initial and all reloading stiffnesses as illustrated in Fig. 3.22. Fig. 3.25 shows the comparison of the initial stiffness (K_1) of all tests, both monotonic and cyclic with moisture content (filled symbols show monotonic results and unfilled symbols show cyclic results). The relevant data sheets are given in Appendix A.4.

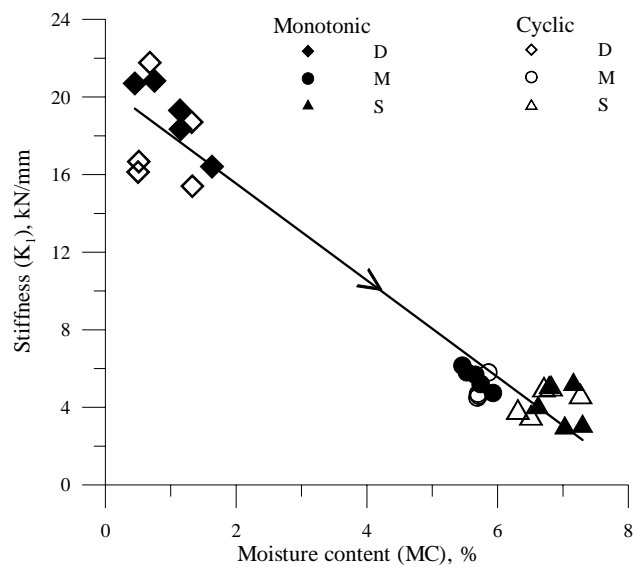


Figure 3.25 Effect of moisture content on the initial loading stiffness

K_1 showed a decreasing trend from dry to saturated condition clustered in three distinct groups.

3.5.4 Effect of Penetration Rate

The penetration rate also influences the behaviour of the soils. Particularly in dry state the behaviour can be affected much more profoundly than in the OMC or saturated states (Fig. 3.22). Thus, the behaviour of the dry specimens at 2.5mm/min and 20mm/min penetration rates for monotonic and cyclic loading are shown in Fig. 3.26. The lower rate (2.5mm/min) caused three distinct stages of material collapse and remoulding (within the entire range of penetration) while the higher rate (20mm/min) caused collapse and remoulding not very distinctly as shown in Fig. 3.26. Therefore, it can be stated that the time available for possible collapse-remoulding operation is low for fast rates. This condition is evident both in monotonic and cyclic experiments.

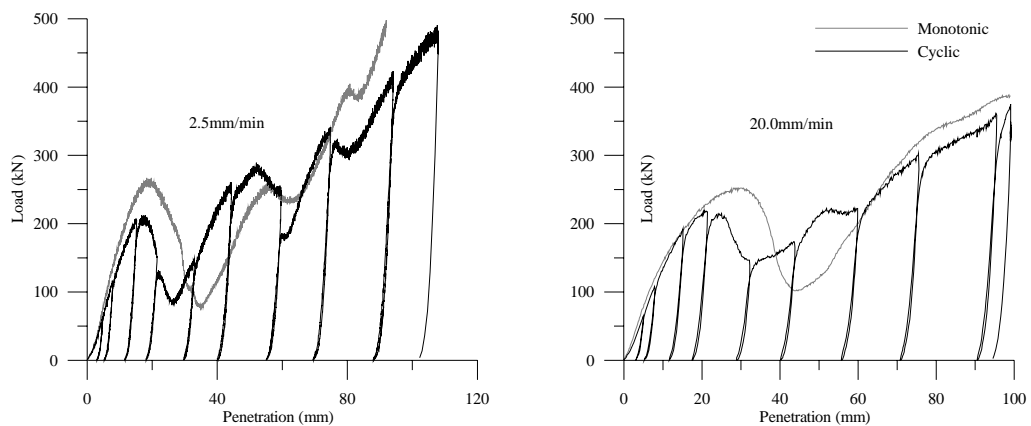


Figure 3.26 Effect of penetration rate

Fig. 3.27 illustrates the comparison of initial stiffness of all tests, both monotonic and cyclic, to the deformation rate (filled symbols show monotonic results and unfilled symbols show cyclic results). The relevant data sheets are given in Appendix A.4.

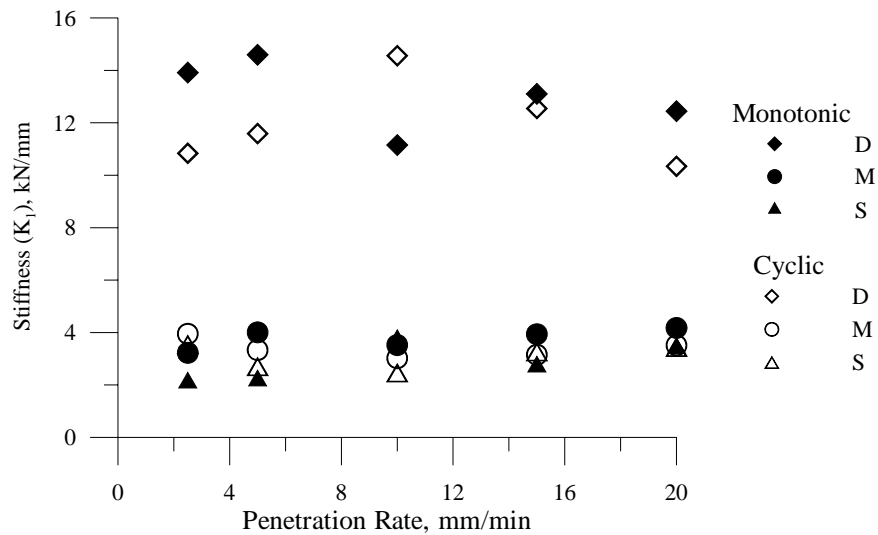


Figure 3.27 Effects of penetration rate on initial stiffness

In contrast, the penetration rate showed little effect on the initial sample stiffness compared to moisture content. However, the trends showed similar patterns of grouping at three distinct plateaus for D (dry), M (OMC) and S (saturated) conditions, where the latter two showed some overlapping.

3.5.4.1 Dimensional Analysis

Dimensional analysis was considered as a tool to differentiate the effect of penetration rate since it was difficult to visualise any marked relationship on the SCT specimens. The relevant data sheets are given in Appendix A.5 and A.6.

By accounting for the important properties a qualitative empirical relationship is established between them in the dimensional analysis (Douglas 1969; Taylor 1974). As such, for the set of experiments conducted, the load obtained (F) was considered as a function of deformation rate (V), dry density of sample (ρ_d) and the permanent deformation (δ) given by

$$F = \oint(V, \rho_d, \delta) \quad (3.6)$$

By assuming an exponential form, Eq. (3.6) is re-written as

$$F = A V^a \rho_d^b \delta^c \quad (3.7)$$

where A , a , b , and c are numerical constants.

Using standard procedure (Douglas 1969; Taylor 1974), the constants a , b , and c have been evaluated as $a = 2$, $b = 1$ and $c = 2$. The relationship when these values are substituted is therefore

$$F = A \rho_d V^2 \delta^2 \quad (3.8)$$

Fig. 3.28 illustrates a typical outcome of the relationship between F and $(\rho_d V^2 \delta^2)$ of monotonic tests at 2.5mm/min penetration rate for dry, OMC, and saturated conditions.

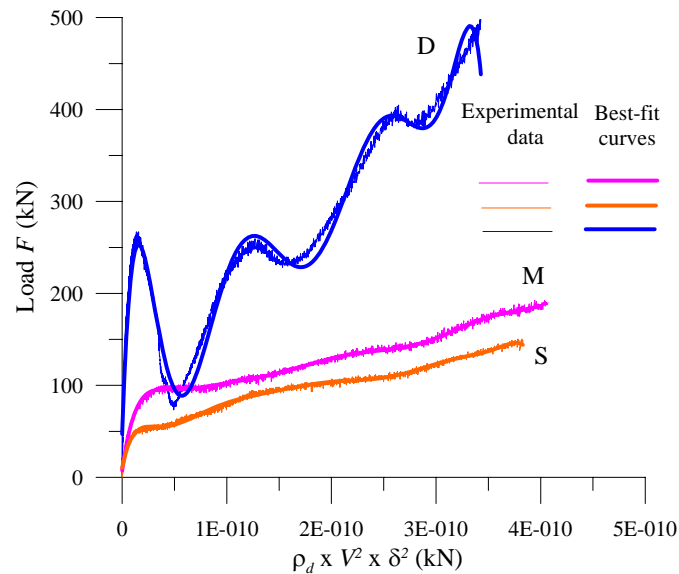


Figure 3.28 Dimensional Relationships of dry, OMC and saturated data

However, the relationship between F and $\rho_d V^2 \delta^2$ is found to best fit with a polynomial of degree 8. The dry sample data exhibited zigzag behaviour as shown in Fig. 3.28.

Therefore, to keep the consistency of all regression relationships, the polynomial order was kept at 8 as it was found to be the best fit for the dry sample data. The expressions obtained are of the form given by

$$F = B + pX + qX^2 + rX^3 + sX^4 + tX^5 + uX^6 + vX^7 + wX^8 \quad (3.9)$$

where $X = (\rho_d V^2 \delta^2)$ and, p, q, r, s, t, u, v, w , and B are numerical coefficients.

The respective relationships between F and $(\rho_d V^2 \delta^2)$ with their best-fit curves for monotonic and cyclic tests are shown in Figs. 3.29 to 3.34. The best-fit constants (p, q, r, s, t, u, v, w and B) and corresponding coefficient of determination R^2 values are located in Appendix A.6. R^2 varied generally between 0.94 and 0.99 suggesting an extremely good fit to the experimental data. However, the anomalies in behaviour patterns in dry conditions are more prominent than that of moist or saturated conditions.

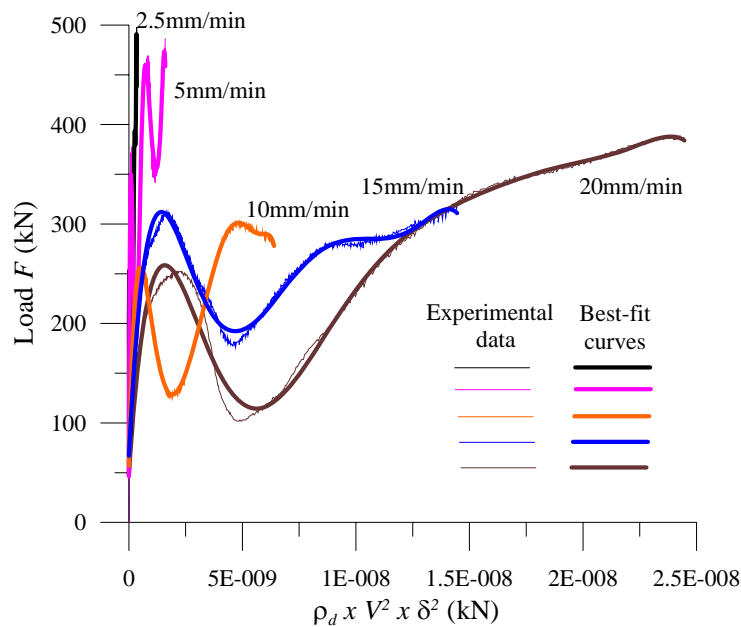


Figure 3.29 Monotonic envelope and best fit curves for dry specimens

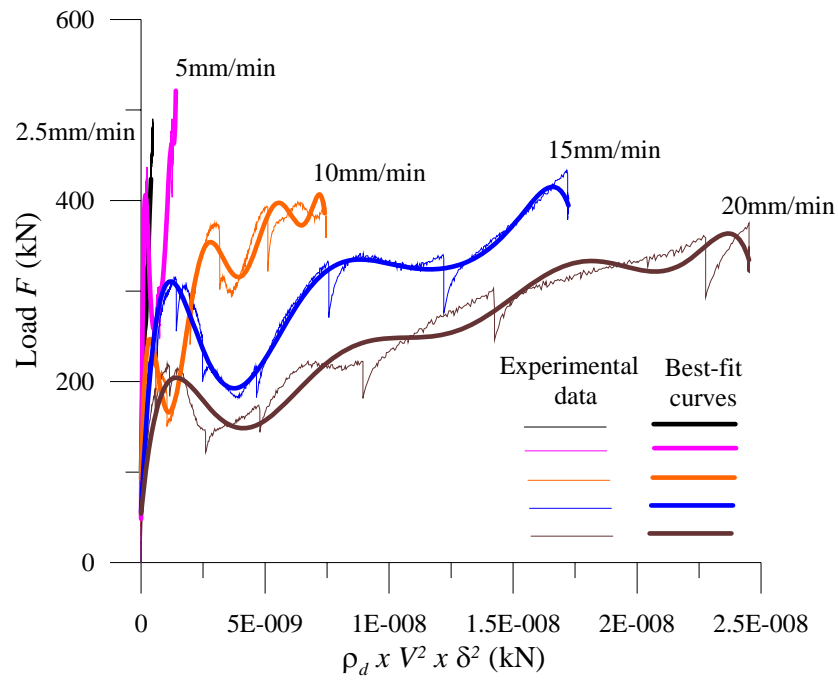


Figure 3.30 Cyclic envelope and best fit curves for dry specimens

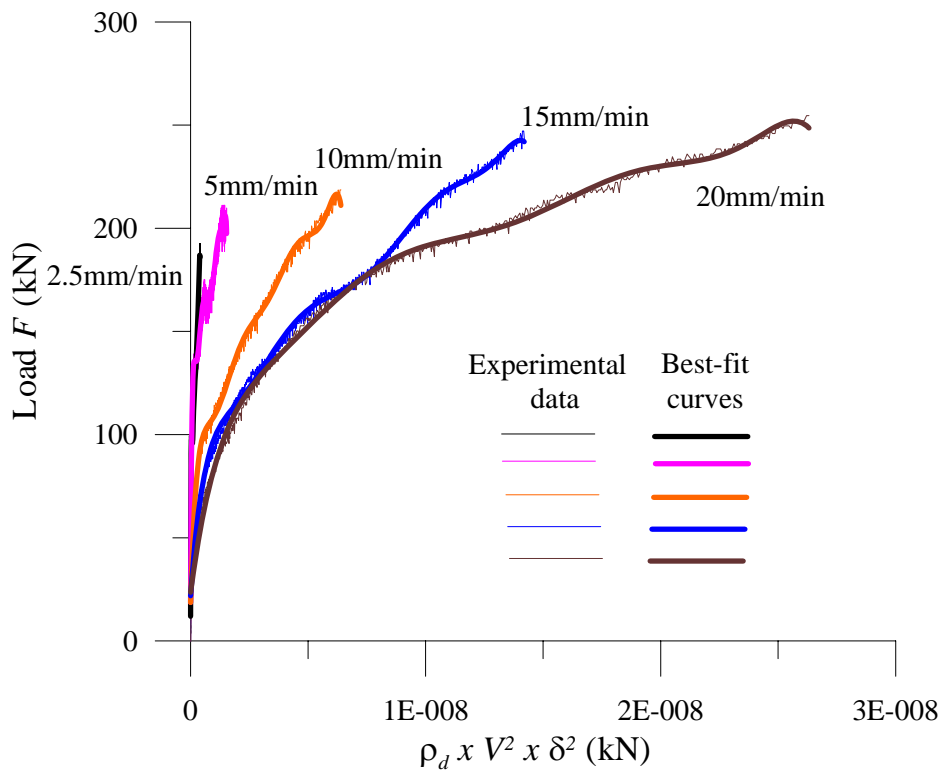


Figure 3.31 Monotonic envelope and best fit curves for OMC specimens

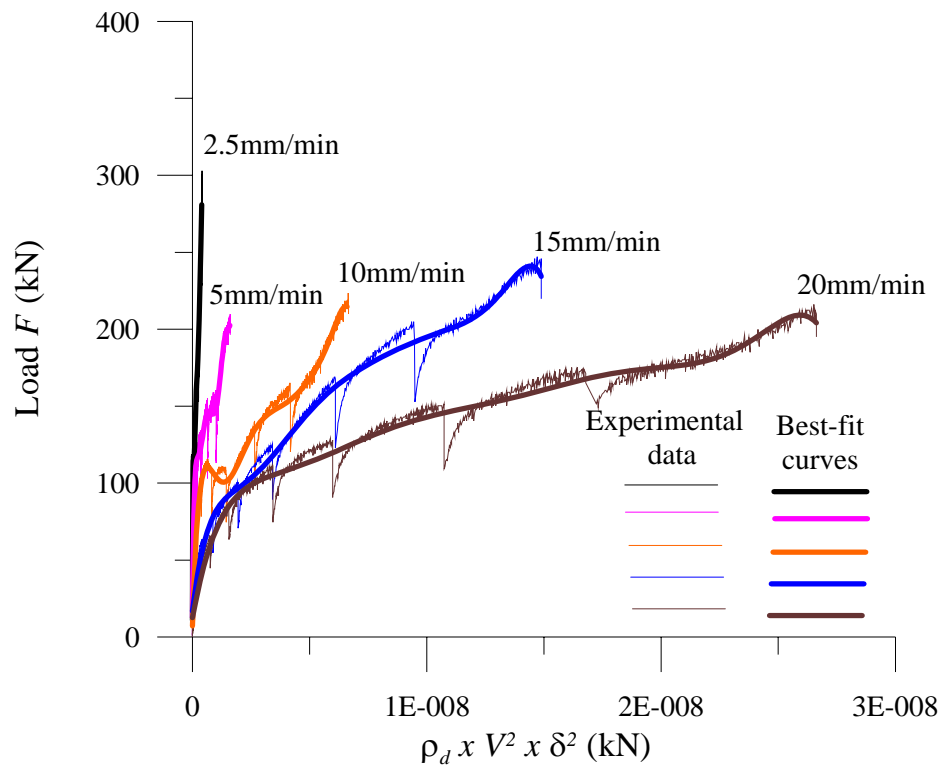


Figure 3.32 Cyclic envelope and best fit curves for OMC specimens

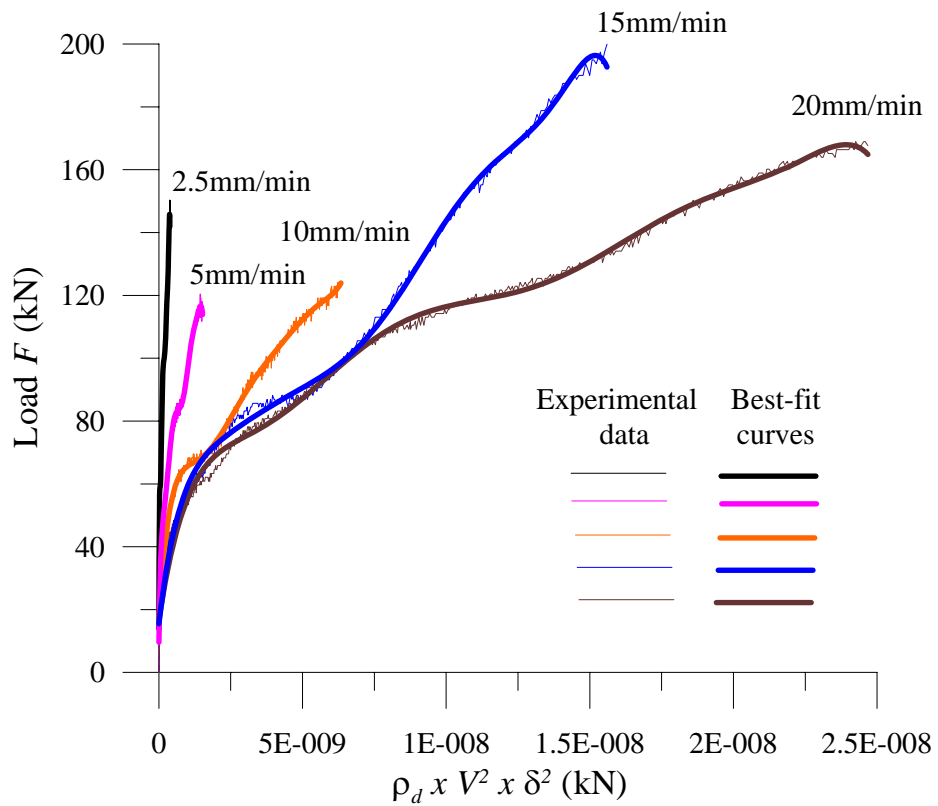


Figure 3.33 Monotonic envelope and best fit curves for saturated specimen

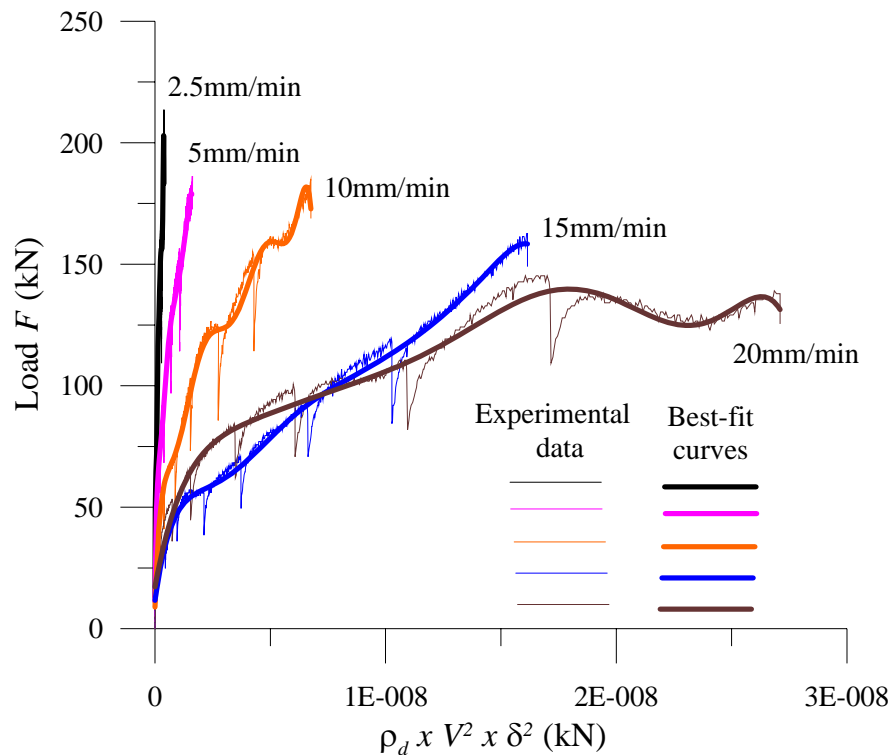


Figure 3.34 Cyclic envelope and best fit curves for saturated specimen

The dimensional analysis has shown the effect of penetration rate more clearly than the load-penetration curves. The higher the penetration rates the lower the limit load response in monotonic and cyclic tests as evident from Figs. 3.29-3.34. However, the sensitivity of load-penetration responses (monotonic or cyclic) due to penetration rates were very much lower compared to that of the moisture levels.

3.5.5 Ternary Plots

A clear and better visualisation of the relationship between the rate of penetration, moisture content and deformation are obtained via ternary plots (Figs. 3.35 and 3.36). Deformations are backcalculated from the above exercise at 25 and 50kN load levels. The loads are considered in the ranges before any secondary effects, i.e., *Stage II* in Fig. 3.13. The effect of each variable is normalised or converted to a percentage. The normalised results for

both monotonic and cyclic tests are located in Appendix A.7. Figs. 3.35 and 3.36 show the ternary plot of the results for monotonic and cyclic loading respectively. Each point in Figs. 3.35 and 3.36 has a (NQ, NF, NL) co-ordinate which denotes the percentage effect of Q, the ratio of rate of penetration to maximum rate of 20mm/min, F, the ratio of sample moisture content to OMC, and L, the ratio of penetrated depth to a deformation of 20mm. The points in Figs. 3.35 and 3.36 are labelled according to the moisture condition of each sample (D = dry, M = OMC and S = saturated).

In both monotonic and cyclic tests, OMC and saturated samples showed little variation in their positions compared to their dry counterparts. The OMC and saturated sample positions are overlapping and clustered towards each other while dry samples are clustered at a different plane altogether which is indicated by a possible boundary shown in Figs. 3.35 and 3.36. This is similar to the trends observed in stiffness calculations (Figs. 3.22, 3.25 and 3.27).

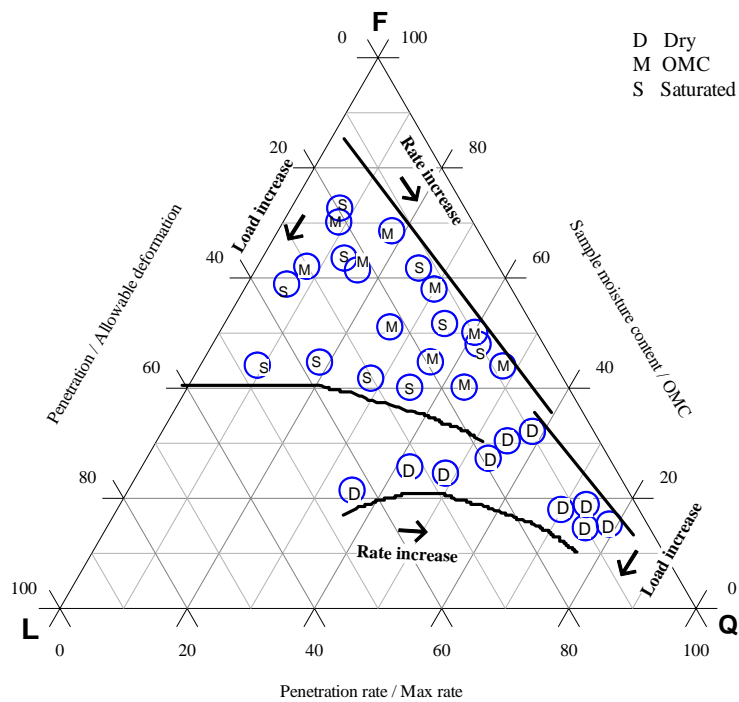


Figure 3.35 Relationship between the moisture content, rate of penetration and penetrated depth in monotonic tests

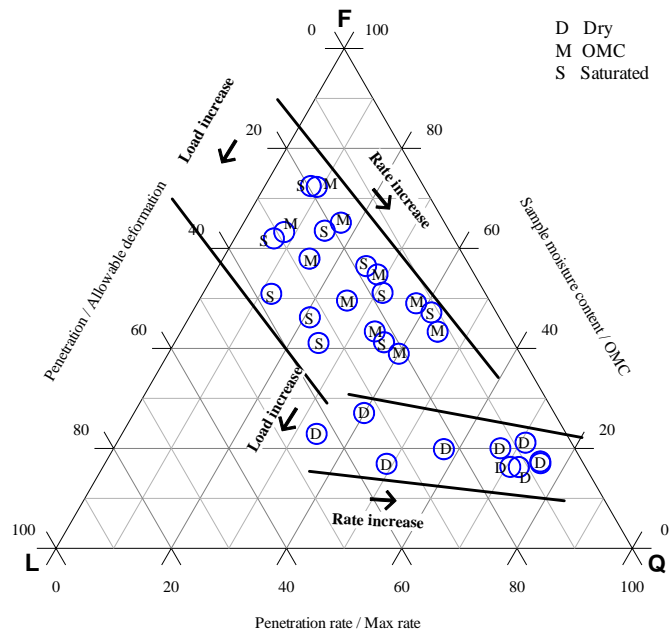


Figure 3.36 Relationship between the moisture content, rate of penetration and penetrated depth in cyclic tests

Thus it could be summarised that to establish material properties through the finite element based backcalculation procedure (described in Chapters 4 and 5), it is sufficient to group the test specimen data according to the moisture level in the specimens. This grouping would be adequate as all the variations expected in the experiments are profoundly described by the upper and lower boundary envelopes of the three groups for this very limited set of test data.

3.6 Summary

This Chapter has presented the findings of the laboratory tests undertaken as part of this thesis. Deformation controlled test results have shown a range of responses for the SCT setup specimens. These responses are categorised into hardening, softening and remoulding ranges. In a highly confined environment the specimens have shown an enhanced ability to resist increase in loading and start remoulding with the increase in the level of penetration.

In summary, these results indicate that the test procedure is capable of characterising the material at very high levels of penetration with permanent deformation in the range of 100mm. This will be more than adequate for practical considerations where a 20mm permanent deformation is usually considered excessive in a railway subgrade, calling for major remediation maintenance. The broad range of stress levels considered in the experiments provided more valuable qualitative and quantitative data than a single or narrow range of stress levels.

The dimensional analysis has shown the effect of penetration rate which otherwise is very difficult to visualise from load-penetration results. The higher the penetration rates the lower the limit load response in monotonic and cyclic tests. However, the sensitivity of load-penetration profiles to penetration rate was low compared with moisture levels irrespective of the type of loading (monotonic/cyclic) as shown in Fig.3.20.

In order to establish material properties from the testing procedure adopted, finite element modelling based back-calculation is used and will be discussed in Chapters 4 and 5. As discussed in Section 3.5.2, with caution based on the limited number of sample tested, the gross simplification of the three groups of dry (Ave m/c = 0.95%), OMC (Ave m/c = 5.7%) and saturated (Ave m/c = 6.85%) states of the material would be adequate in defining the material properties sought in a railway substructure. This is justifiable considering the vast variations in soil properties spatially even within relatively small distances in the field and their behaviour over a wide range of stress states and their mineralogical compositions (Murphy 1987).